



1 **Global basic landform units derived from multi-source digital elevation**
2 **models at 1 arc-second resolution**

3 Xin Yang^{1,2,4†}, Sijin Li^{1,2,4†}, Junfei Ma^{1,2,4}, Yang Chen^{1,2,4}, Xingyu Zhou^{1,2,4}, Fayuan Li^{1,2,4}, Liyang Xiong^{1,2,4}, Chenghu
4 Zhou³, Guoan Tang^{1,2,4*} & Michael E. Meadows^{5,6*}

5 † These authors contributed equally to this work.

6 * Co-corresponding authors: Guoan Tang tanguoan@njnu.edu.cn; Michael E Meadows michael.meadows@uct.ac.za

7 ¹School of Geography, Nanjing Normal University, Nanjing, 210023, China

8 ²Key Laboratory of Virtual Geographic Environment (Nanjing Normal University), Ministry of Education, Nanjing,
9 210023, China

10 ³Institute of Geographical Information Science and Natural Resources, Chinese Academy of Science, Beijing, 100101,
11 China

12 ⁴Jiangsu Centre for Collaborative Innovation in Geographical Information Resource Development and Application, Nanjing
13 210023, China

14 ⁵School of Geography and Ocean Sciences, Nanjing University, Nanjing 210023, China

15 ⁶Department of Environmental & Geographical Science, University of Cape Town, Rondebosch 7701, South Africa

16



17 **Abstract.** Landforms are fundamental components of the Earth surface, providing the base on which surface processes operate.
18 Understanding and classifying global landforms, which record the internal and external dynamics of the planet's evolution,
19 constitutes a critical aspect of Earth system science. Advances in Earth observation technologies have enabled access to higher
20 resolution data, for example remote sensing imagery and digital elevation models (DEMs). However, landform data with a
21 resolution of approximately 1 arc-second (approximately 30 m) are lacking at the global scale, which limits the progress of
22 geomorphologic studies at finer scales. Here, we propose a novel framework for global landform classification and release a unique
23 dataset called Global Basic Landform Units (GBLU), which incorporates a comprehensive set of objects that constitute the range
24 of landforms on Earth. Constructed from multiple 1 arc-second DEMs, GBLU ranks among the highest-resolution global
25 geomorphology datasets to date. Its development integrates geomorphological ontologies and key derivatives to strike a balance
26 between mitigating local noise and preserving valuable landform details. GBLU categorizes the Earth's landforms into three levels
27 with 26 classes, yielding discrete vector units that record landform type and distribution. Comparative analyses with previous
28 datasets reveal that GBLU enhances capture of landform details, enabling more precise depiction of geomorphological boundaries.
29 This refinement facilitates the identification of novel spatial disparities in landform patterns, exemplified by marked contrasts
30 between Asia and other continents, and highlights the distinct prominence of China in terms of landform diversity. Given that the
31 fundamental data resolution of GBLU accords well with available remote sensing datasets, it is readily incorporated into analytical
32 workflows, exploring the relationship between landforms, climate and land cover. The full data set is available on the Deep-time
33 Digital Earth Geomorphology platform and Zenodo (Yang et al., 2024; <https://doi.org/10.5281/zenodo.13187969>).

34 1. Introduction

35 Approaches to geomorphology vary, and include research on, for example, processes, materials, hazard and risk, and
36 chronology, but the essential basis of all of these studies is the *landform* (Evans, 2012), which can be regarded as the 'final surface
37 status' resulting from the combined influence of various forces. The morphology of landforms and their associated evolutionary
38 processes have long been a source of fascination, leading ultimately to the development of the formal science of geomorphology
39 (MacMillan and Shary, 2009). Classifying and mapping the Earth's surface into landform types according to morphological
40 characteristics is a primary means of understanding surface patterns and processes on planet Earth (Evans, 2012; Xiong et al., 2022)
41 and advancement in this field has potential benefits for the more efficient allocation of global resources to promote sustainable
42 development (Dramis, 2009).

43 Traditional landform mapping primarily relies upon manual interpretation based on the topographic maps and aerial
44 photographs supported by field investigations (Drăguț and Blaschke, 2006; Hammond, 1954; Iwahashi et al., 2018; Pennock et al.,
45 1987). However, a series of technological developments has facilitated the automation of landform classification in recent decades,
46 largely dependent on topographic derivatives calculated from DEMs, such as slope, aspect, relief, curvature, roughness (Amatulli
47 et al., 2018; Dyba and Jasiewicz, 2022; Jasiewicz and Stepinski, 2013). With the development of earth observation systems and



48 DEM refinement, several global landform datasets based on this framework have been proposed using various data sources and at
49 different levels of spatial resolution (Florinsky, 2017; Iwahashi and Yamazaki, 2022). Using a decision tree algorithm and 1-km
50 SRTM30 data, Iwahashi and Pike (2007) generated a global terrain classification gridded dataset containing 16 undefined
51 topographic types determined by slope gradient, local convexity, and surface texture. Relying on elevation and the standard deviation
52 of elevation, Drăguț and Eisank (2012) adopted an object-based method to automatically classify global landforms from SRTM data
53 resampled to 1 km. Meanwhile, Iwahashi et al. (2018) improved their previous work and established 15 landform classes based on
54 MERIT DEM. To further eliminate issues involved in detecting narrow valley bottom plains, metropolitan areas, and slight inclines
55 in otherwise largely flat plains, Iwahashi and Yamazaki (2022) introduced the elevation above the nearest drainage line measure,
56 and achieved landform classification based on a DEM at 90m resolution. However, as the authors stated, unsupervised classification-
57 based methods to perform higher-resolution global landform classification require an international team with knowledge of
58 geomorphological development in a variety of climatic and physiographic settings. In addition, at regional and/or global scales,
59 several researchers have achieved automated landform classification following the Hammond procedure (Gallant et al., 2005;
60 Karagulle et al., 2017; Martins et al., 2016). All these datasets have provided valuable resources to explore surface patterns, and
61 also played important roles in supporting related disciplines such as hydrology, pedology, and ecology among others.

62 However, shortfalls remain in current landform classification research and require attention to the following points. Firstly,
63 previous studies have adopted relatively coarse resolution DEMs, resulting in an inaccurate depiction of topographic information.
64 Recent developments in Earth observation technology have concentrated on the deployment of digital elevation models (DEMs),
65 which contain abundant geometric information about surface relief (Drăguț and Eisank, 2011), although the approach and methods
66 of implementing landform classification have not kept pace with advances in DEM resolution and quality. Nevertheless, higher
67 DEM data resolution can be regarded as a double-edged sword, in that it at once provides the opportunity for landform mapping at
68 a finer scale while at the same time increasing the challenge of reducing the noise effect (Jasiewicz and Stepinski, 2013) and
69 maintaining the integrity of the identified landforms. Secondly, at the global scale, diverse and complex environmental factors have
70 shaped different types of landforms that pose substantial challenges to the generalizability of classification methods (Li et al., 2020).
71 With increasing human impact on landforms, a re-evaluation of landform classification that takes advantage of an increasingly
72 potent digital database and ongoing improvements in human understanding of landform evolution and processes seems opportune.
73 Finally, landform information obtained from a particular metric is derived at a particular spatial scale, determined jointly by the
74 DEM resolution and window size in the neighborhood analysis, giving rise to uncertainties in the landform classification results.

75 Therefore, the development of innovative classification approaches and systems based on high resolution DEMs remains a
76 priority for research on global landforms. In this study, we conduct a classification and mapping of global landforms based on a
77 DEM at 1 arc-second resolution. We focus on the classification of basic landforms that emphasizes morphological differences and,
78 in so doing, we present the practical expression of landform ontology at the global scale that offers valuable insights into the Earth's
79 surface structure comprising the constellation of landform types and their boundaries. The objectives of this research are: (1) to



80 construct a global classification system for landforms that integrates geomorphological knowledge, (2) to design a novel framework
81 for global basic landform classification, (3) to develop an automated classification and mapping model for global landforms, and
82 (4) to make available a comprehensive high-resolution dataset of global landform units.

83 **2. Methodology**

84 **2.1 Hierarchical classification system and data**

85 In aiming to provide a comprehensive classification of landforms at the global scale, our study encompasses all terrestrial
86 regions worldwide, including islands and polar areas. Identifying landform objects and constructing a classification system is a
87 preliminary and significant step in geomorphological and landform classification studies. It is crucial to recognize that landforms
88 not only represent assemblages of quantitative characteristics but also convey the basic human understanding of nature (Smith and
89 Mark, 2001). For example, the identification of what is acknowledged as a ‘mountain’ is as much a product of human perception as
90 of its natural characteristics (Smith and Mark, 2003), thus emphasizing the importance of incorporating human understanding into
91 landform classification and mapping. Therefore, we focus here on the classification of basic landforms that emphasizes
92 morphological differences that are not only perceptible to humans but also constitute vital components in the analysis of surface
93 environments. In taking into consideration the complexity of global landform characteristics, the classification criteria should satisfy
94 the following requirements: (1) the determined classes should be globally applicable; (2) the setting of the landform types should
95 conform with the current knowledge domain of geomorphology; and (3) specific criteria should be able to be interpreted and applied.
96 In employing existing landform classification principles (Zhou et al., 2009), here we propose the set of criteria for basic landform
97 classification. The new criteria integrate the typical rules of landform classification with indices proposed in this work, and are
98 aimed at reflecting human knowledge in a quantitative way. We establish a hierarchical classification system comprising 3 levels
99 and 23 classes (Table A1), thereby advancing a structured framework for understanding Earth's diverse landscapes. The first-level
100 (L1) types are defined as ‘plain’ and ‘mountain’, reflecting the most fundamental morphological characteristics of landforms. Plains
101 and mountains are the most direct reflection of the combined effects of geomorphological processes and profoundly influence
102 biological activities. This classification perspective aids researchers in conducting macro-scale studies. At the second level (L2),
103 plain landforms retain their labels to guarantee completeness of the classification system, and are further divided into low-altitude,
104 middle-altitude, high-altitude, and highest-altitude plains based on elevation. Mountains are subdivided at L2 into hills and other
105 mountains with varying degrees of relief. At L3, we provide a further detailed classification of hills and mountains based on elevation.
106 To attain global coverage, we utilize three DEM datasets (Table 1). These datasets are publicly available for access and have
107 been widely used in geomorphological studies, ensuring their accuracy and validity. In this work, the ‘Forest and Buildings removed
108 Copernicus DEM’ (FABDEM) (Hawker et al., 2022) is the primary data for latitudes 60°S-80°N. This dataset is the first bare-earth
109 DEM dataset at a global scale at 1 arc-second (approximately 30-meter) resolution, developed using machine learning techniques
110 from Copernicus DEM. By eliminating the bias resulting from building and vegetation heights, some terrain features, such as slope,



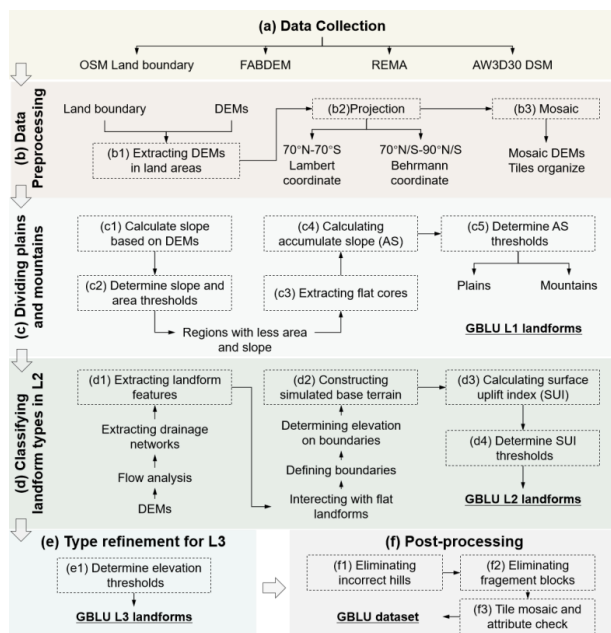
111 aspect, and watersheds, can be estimated more accurately, which is of significant benefit in landform classification. Meanwhile, the
 112 Advanced Land Observing Satellite (ALOS) World 3D - 30 m (AW3D30) (Tadono et al., 2014) dataset is used to supply data for
 113 the area the missing from FABDEM. In addition, to avoid the negative impact of ocean pixels on landform classification results, the
 114 OpenStreetMap (OSM) Land Polygon was utilized as a mask to eliminate the sea.

115 **Table 1. Data sources and attributes**

	FABDEM	AW3D30 V3.2	REMA
Spatial Coverage	60°S-80°N	82°S-82°N	56°S-88°S
Spatial Resolution	1 arc-second	1 arc-second	32 m
Vertical Accuracy	<4 m	4.4 m (RMSE)	4 m (RMSE)
Release Date	2021	2021	2022
Data link	https://data.bris.ac.uk/data/datas/et/s5hqmjcdj8yo2ibzi9b4ew3sn	https://www.eorc.jaxa.jp/ALOS/jp/dataset/aw3d30/aw3d30_j.htm	https://www.pgc.umn.edu/data/rema/

116 **2.2 Global landform classification method**

117 In this study, we propose a knowledge-guided framework and provide the corresponding implementation workflow. The
 118 proposed method of global landform classification has a hierarchical structure, involving data pre-processing, identification of
 119 mountains and plains, calculation of the mountain uplift index (SUI), landform classification, and post-processing. Figure 1
 120 illustrates the workflow. The following sections provide details that should allow users to reproduce our results. In this study, we
 121 built factor calculation and landform classification models based on tools in ArcGIS Pro. A detailed description of the step-by-step
 122 procedures follows below.



123
 124 **Figure 1. Workflow for global landform classification used in this study.**

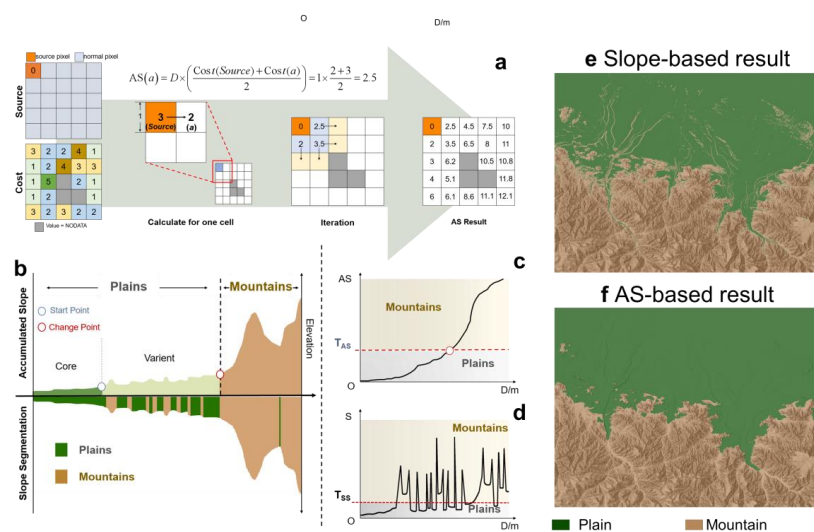


125 **2.2.1 Data pre-processing**

126 As shown in Figure 1b, data pre-processing focuses primarily on land area extraction and data merging. We use the OSM
 127 land polygon as the land mask to eliminate the marine pixels that negatively influence subsequent processes. To improve processing
 128 efficiency, the original DEM elements with size of 1×1 degree are mosaiced to tiles of 10×10 degrees. Meanwhile, due to the
 129 requirement of calculating landform derivatives, we determine the projection principles as follows: data from latitudes below 70°
 130 are transposed onto the Behrmann projection, and the remaining data are transported onto the Lambert azimuth equal-area projection.

131 **2.2.2 Identifying plains and mountains**

132 Landforms represent the most fundamental elements of the Earth’s terrestrial surface and reflect both internal and external
 133 forces acting over time. Identifying and distinguishing contrasting plains and mountains represents the initial step in basic landform
 134 classification and mapping. We have designed a practical framework based on landform ontology to classify plains and mountains.
 135 The plains can be separated into core, transition and boundary, whereby the core represents areas with the most typical flat
 136 characteristics, i.e. very low relief. Transitions have plain cores but also contain sloping elements, i.e. areas that in part satisfy their
 137 classification as plain but also exhibit sloping characteristics not typical of plain. Misclassifications usually occur in transition areas
 138 due to their atypical characteristics. Meanwhile, the boundary represents the part of the plain area where the geomorphological
 139 semantics and labels change to the mountain.



140
 141 **Figure 2. Illustration of calculation methods.** **a** schematic diagram of the cost-distance algorithm. **b** profile reflecting landform
 142 composition according to the proposed conceptual model of plains, segmented based on the slope; **c** calculated result of the AS and
 143 **d** calculated result of slope, where T_{AS} is the threshold of AS, and T_{SS} is the threshold of surface slope. For Figures 2c and d, areas
 144 smaller than the threshold are classified as plains (marked in green), while the remaining areas are classified as mountains (marked
 145 in brown). **e** and **f** comparison of the AS and slope indicators in the division of plains and mountains.

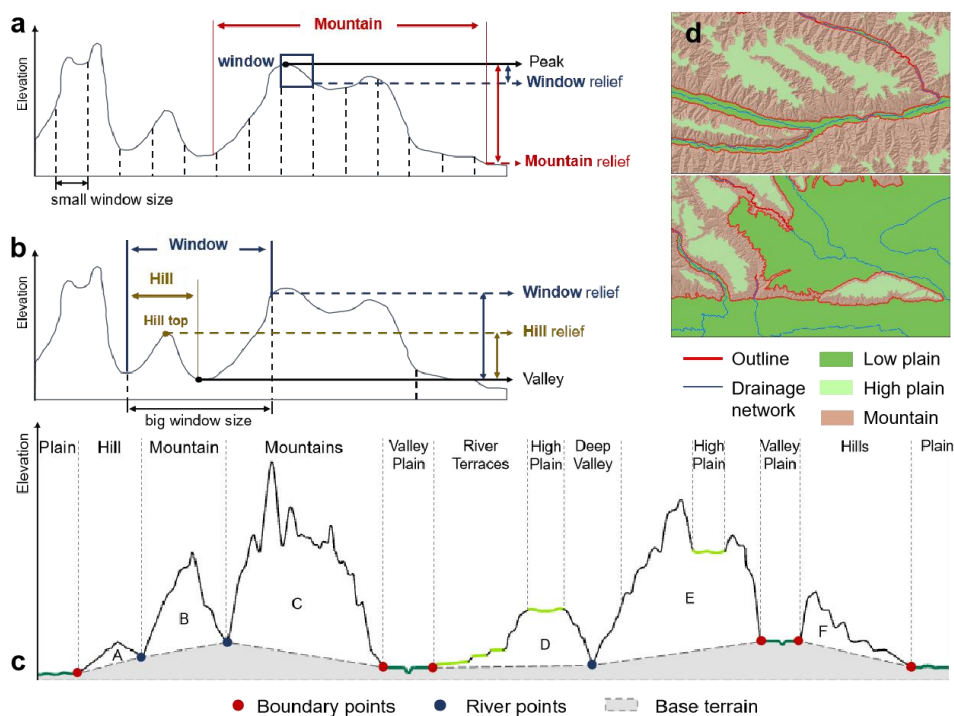
146 Firstly, we regard the areas with low slope angles as the plain cores. Here, the slope threshold (T_1) is recommended to be
 147 set as 1.5-3 degrees according to our global pre-assessment experiments. Areas where the slope angle lies below the threshold T_1
 148 are classified as plain cores. Secondly, we employ the accumulated slope (AS) as representing the different slope attributes of



149 landforms. The AS is calculated as the minimum cumulative cost of each position to the nearest landform core along a specific path
150 (Sechu et al., 2021). The algorithm follows the geospatial analysis principle whereby the lowest cost is computed through the
151 creation of least-cost paths between cores and general positions. The tool of distance accumulation in ArcGIS Pro can achieve this
152 calculation. In its implementation, this algorithm employs an iteration starting from the cell closest to the cores and follows the
153 calculation principle shown in Figure 2a to compute the minimum cumulative cost of each cell to the core. The completed area is
154 then expanded until all grids are associated with increasing costs. Segmenting landforms through the determination of the thresholds
155 for landform derivatives is one of the most common methods used in geomorphological studies and achieves the most direct
156 integration of geomorphological knowledge and expertise. As shown in Figure 2b, due to differences in topographic characteristics
157 between plains and mountains, the AS has a low rate of increase in the areas classified as plains and a high rate of increase in rugged
158 areas. This phenomenon reduces the difficulty of determining an appropriate AS threshold, which can be achieved by searching for
159 abrupt changes in the AS profile. In this step, taking into consideration the geomorphological perspective, the threshold of AS (T_2)
160 is recommended to be 1500-2000 based on the pre-experimental results conducted on numerous samples worldwide. This threshold
161 range is provided as a reference, but needs to be determined by integration with expert knowledge within different geomorphic
162 regions. In some cases, it may exceed the recommended threshold range. Areas where the AS value is less than T_2 are regarded as
163 plains, and the remaining areas are mountains. Through the above segmentation, we can obtain the boundary of plain and construct
164 the complete plain area consisting of core, variant and boundary. As shown in Figures 2e and f, this novel workflow exaggerates the
165 difference between the plains and mountains and converts the local slope into an indicator of global landform characteristics. This
166 novel method avoids the negative effect of local window analysis and is beneficial for maintaining the landform semantics for each
167 block.



168 2.2.3 Classifying landform types in level 2



169
170 **Figure 3. Uncertainty in relief calculation based on the window analysis.** a and b the relationship between different windows
171 and topographical relief. c schematic diagram illustrating the base terrain of mountains. d features used to create TIN and build base
172 terrain.

173 Then, we focus on the differences of terrain relief to achieve the comprehensive classification of L2 landforms. Terrain
174 relief refers to the difference in elevation between the highest and lowest points within a particular spatial unit. This factor
175 significantly influences landform classification. However, commonly employed indices reflecting topographic relief are achieved
176 using a window of fixed size such as 3×3, 5×5 pixels, or larger (Maxwell and Shobe, 2022), a method that fails to account for
177 geomorphological semantics, and which therefore disregards the integrity of a mountain. Window size has a significant impact on
178 results of relief calculation. As shown in Figures 3a and b, window analysis tends to disrupt the integrity and continuity of
179 geomorphological elements. Moreover, a small window size is insufficient to capture the entire mountain, particularly in the case
180 of large mountains, while a large window size may incorporate other mountains and fail effectively to capture the relief. The
181 uncertainty introduced by window size further increases the difficulty of global classification and mapping based on relief. Therefore,
182 we propose a new method for surface relief calculation.

183 In quantitative analysis, it is crucial to consider the underlying terrain of mountains to accurately assess changes in elevation.
184 According to the above consideration, we construct mountain units as fundamental analysis units and propose a novel derivative
185 named the surface uplift index (SUI). In this paper, surface relief is defined as the degree of uplift relative to the flat areas surrounding
186 the mountains. We regard the elevation at the foot of the mountain as the base elevation and then calculate the elevation difference



187 between each position on the mountains and the base elevation. Compared to the traditional method of relief calculation (e.g.,
188 difference in elevation within a particular window size), SUI considers the vertical elevation differences between the surface and
189 the mountain base, which is more consistent with the human perception of mountain morphology.

190 This step includes three sub-procedures. Firstly, we constructed the unit ‘rugged’ and associated fluvial features based on
191 the boundary of plain. The plain boundary then lies at the foot of landforms classified as mountain. However, when the area of the
192 mountain is large, and the base elevation is constructed only on basis of the plain boundary, the result may be inaccurate. To refine
193 the representation of surface relief, we also take into account linear features representing the rivers. These additional lines can be
194 obtained through DEM based hydro-analysis (Li et al., 2021). In order to ensure that plains at high elevations do not interfere with
195 the definition of the mountain unit, since these are, in effect, part of the mountain range (Figure 3c) we exclude high elevation plains
196 that have no fluvial features to retain the integrity of the associated mountain range. Figure 3d shows the elements involved in
197 establishing the base elevation, which corresponds to the boundary of the low altitude plains and fluvial features (marked in red in
198 Figure 3d), therefore excluding high altitude plains (marked in light green in Figure 3d). Secondly, we constructed the base elevation
199 to underpin the calculation of the SUI. In this case, the rugged unit replaces the analysis window. In this step, we constructed the
200 triangulated irregular network (TIN) based on the position extracted in the first step and then regard these TIN data as the base
201 elevation. The construction of TIN can be achieve in ArcGIS Pro through create TIN. Thirdly, the SUI is obtained by calculating
202 the difference between each cell height and its corresponding base elevation. This novel method provides a more appropriate
203 representation of the underlying terrain.

204 **2.2.4 Type refinement for L3**

205 According to the results of previous studies (Zhou et al., 2009), we constructed the classification criteria shown in appendix
206 of Table A1. For the plains, we use altitudes of 1000m, 3500m and 5000m as break points to generate low-, middle-, high- and
207 highest-altitude landforms. Mountains are classified as hill, low-relief, middle-relief, high-relief, and highest-relief mountains, based
208 on threshold SUI values of 200m, 1000m, 3500m and 5000m. In all, this yields 6 L2 and 23 L3 classifications.

209 **2.2.5 Post-processing**

210 Following completion of the above processes, a map is generated that includes all the basic landform units. However, due
211 to interference caused by the existence of locally steep changes in topographic relief, this output still contains some features in the
212 plain areas misclassified as hills. Meanwhile, although the data we used are of high resolution and good quality, outliers and/or data
213 noise remain. Such anomalies may result in small landform blocks with relatively low terrain relief and, in accommodating this,
214 we designed an optimization process to correct hill misclassification. We used area and SUI as reflecting their characteristics (e.g.
215 fragmented and relatively low relief). Considering the application of landform data in geomorphologic mapping and the resolution
216 of basic data, we determined that our study corresponds approximately to the equivalent of 1:200,000 geomorphological mapping.
217 Under the conditions of 1:200,000 scale, the minimum displayable patch size is approximately 0.16 km². The SUI threshold is
218 derived from (Zhou et al., 2009), which defines plains as the blocks with relief of less than 30 metres. Therefore, blocks with areas



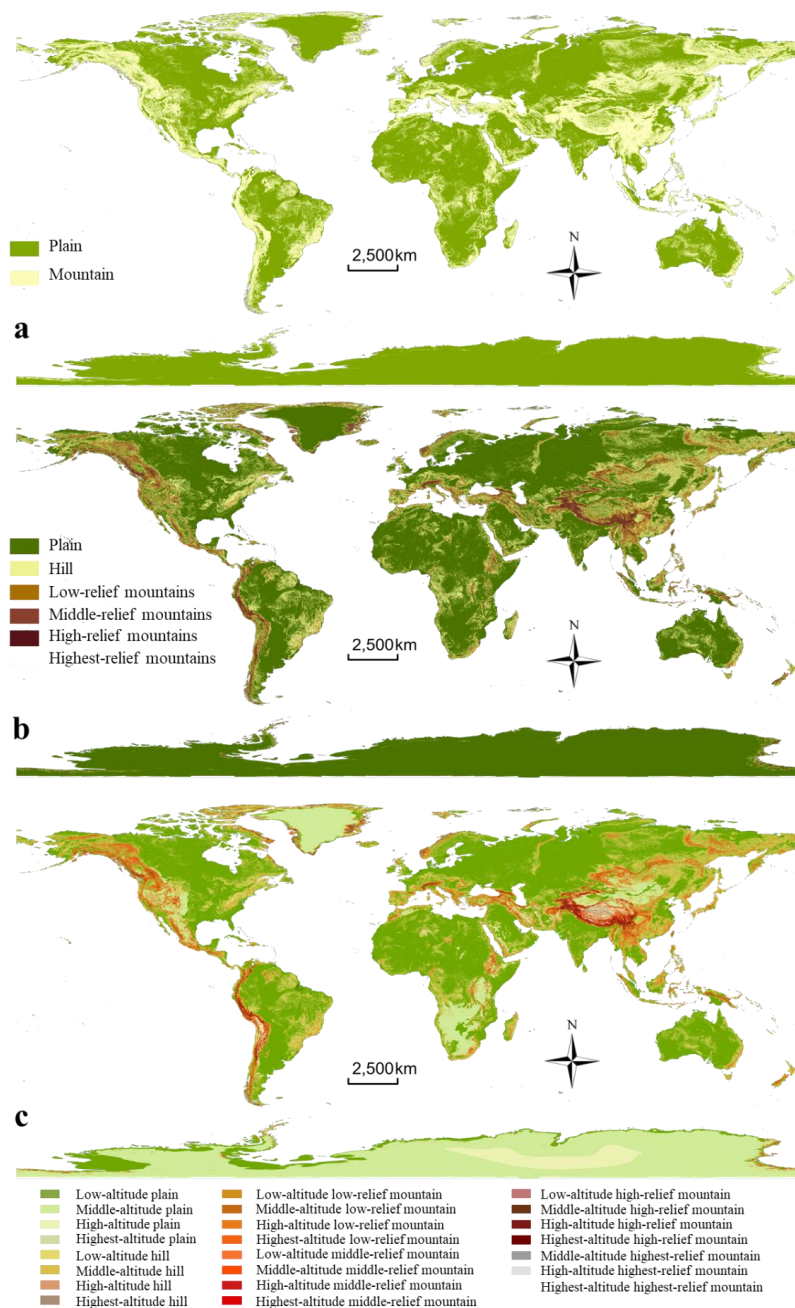
219 of less than 0.16 km^2 and SUIs below 30 metres are regarded as misclassified blocks which are then integrated as part of the
220 surrounding plains.

221 Meanwhile, we designed an additional step to optimize the results for desert areas. Many arid regions are characterized by
222 dunes, which are distinctive aeolian landforms of varying shape and size constructed from unconsolidated sand (Hugenholtz et al.,
223 2012). Dunes are generally smaller in scale than mountains and this challenges our approach to basic landform mapping (Shumack
224 et al., 2020), increasing the difficulty of accurate dune mapping. In this study, we regarded sand dunes as hills due to their
225 morphological similarity. However, due to the variation of dune size and shape, it is challenging to correctly classify these dunes as
226 hills according to our proposed method. Therefore, we design an optimization step to correct the classification results in which dunes
227 and inter-dune areas are separated and identified according to their altitude and SUI. Firstly, on the basis of on their
228 geomorphological characteristics, remote sensing images, and hillshade maps, we demarcated the major global sand desert regions.
229 Secondly, we used the DEM to extract the topographic feature lines by surface analysis of extracting desert feature lines. Employing
230 the SUI calculation as for other regions, we then constructed the base terrain, in this case, the river networks were extracted with
231 the threshold T_{D1} of 20000, and then we extracted sampling points from these networks to construct TINs. We calculated the SUI
232 and then set the segmented threshold T_{D2} . Due to inconsistencies in the scale of dunes worldwide, we applied an adjustable T_{D2}
233 ranging from 2m to 10m. Areas less than T_{D2} are defined as inter-dunes (equivalent to plains in the basic landform classification).
234 All patches smaller than T_{D3} 0.02 km^2 were regarded as fragments and integrated into the surrounding vector blocks. Finally, we
235 employed the smoothing tool to ensure appropriateness of the landform boundary.



236 **3 Results and discussion**

237 **3.1 Global landform classification results**



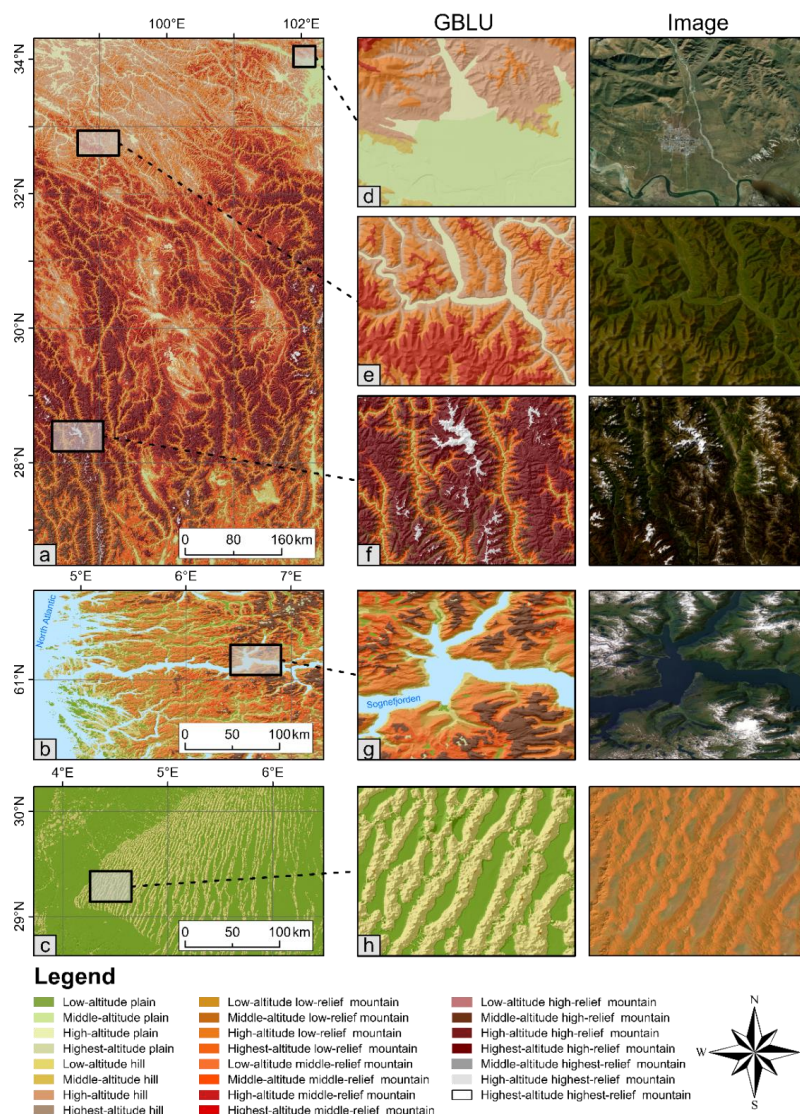
238

239 **Figure 4. Results of the basic global landform classification with 30 m resolution. a, b and c represent the L1, L2 and L3**

240 landforms, respectively.



241 Figure 4 shows the global landform classification results based on the abovementioned framework. This hierarchical dataset
242 provides a more comprehensive understanding of the Earth surface. To visualize the results in detail, three typical regions
243 selected to demonstrate the performance of the GBLU dataset. Figure 5 shows the GBLU in typical regions and corresponding
244 remote sensing image from Esri world imagery. The selected regions contain examples of the main landforms on Earth, as well as
245 transition areas of different landforms. In the mountainous areas as shown in Figure 5a, mountain range and valley orientation is
246 clearly discernible. The GBLU clearly illustrates the transition zones between mountains and plains, as well as potential floodplains.
247 While such phenomena are visually discernible in remote sensing imagery, using our proposed framework, they are extracted based
248 on quantified morphological characteristics. The abundant textural information provided by GBLU can facilitate study of areas with
249 high geomorphological value, such as fjords (Figure 5b). In desert areas Figure 5c, GBLU effectively illustrates the transitional
250 patterns between dunes and depressions. Based on abundant morphological characteristics, GBLU can depict sand dune boundaries
251 that are strikingly consistent with those visible in imagery. This further underscoring the performance of GBLU in capturing detailed
252 geomorphic features across varied terrains.



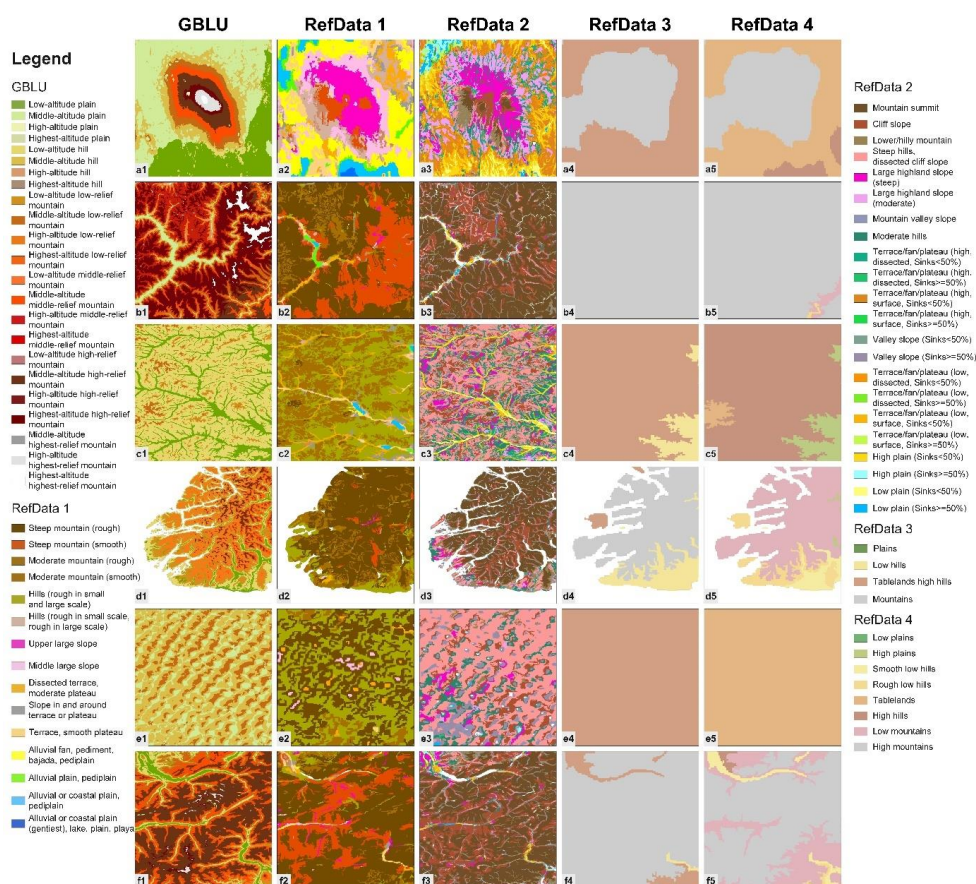
253
 254 **Figure 5. Comparison of landform classification results and remote sensing imagery.** a eastern part of the Tibetan Plateau. b
 255 the Fjord coast in western Norway. c desert area in the central Sahara. e-h are local enlarged areas.

256 3.2 Result comparison and validation

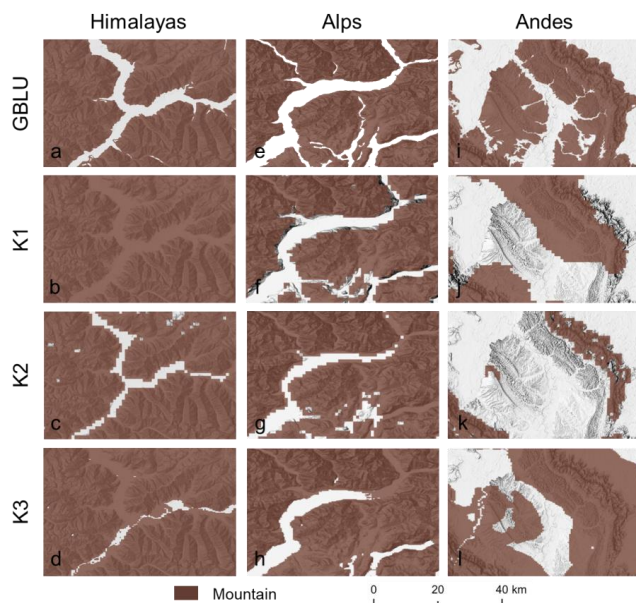
257 We conducted comparisons between the GBLU dataset and multiple other datasets to comprehensively evaluate our
 258 results. Specifically, we compared the outcomes of five landform classifications across a range of sample areas. The most
 259 significant improvement achieved by applying GBLU is the increased detail in representing terrain features. The GBLU-based
 260 landform classification markedly enhances delineation of independent landforms, such as dunes and mountains, which have
 261 clear boundaries and serve as key elements in the analysis of spatial structure and interactions. The classification systems of
 262 RefData 3 and 4 are similar to GBLU but have a coarser resolution of 1 km, making them less effective in capturing terrain
 263 details. Figure 6 illustrates that there is a variation in the understanding of landform types among different scholars. As stated



264 by the authors, RefData1 and RefData2 align more closely with terrain classification systems. Although these categories do
 265 include common landforms such as plain and mountains etc., they also encompass other types of terrain features like slope.
 266 In this paper, we consider landforms of plain or mountain to represent larger scales relative to terrain objects like "slope."
 267 Therefore, in designing the classification system, we think that categorizing 'slope' at the same level as 'plain' or 'mountain'
 268 can lead to some comprehension difficulties. Therefore, GBLU offers a more comprehensive landform classification system
 269 and expresses the integrity of landform objects more closely aligned with the ontological understanding of landforms.



270
 271 **Figure 6. Comparison of GBLU with RefData 1 - 4.** Selected study areas, from top to bottom, are as follows: a. the Kilimanjaro,
 272 b. Namcha Barwa in Himalaya, c. Greater Khingan Mountains, d. Fjords in New Zealand, e. Badain Jaran Desert and f. Central
 273 Alps. Refdata1 is the 15-class global terrain classification created by Iwahashi et al. (2018) based on 280m DEM. Refdata2 is the
 274 The 22-class global terrain classification created by Iwahashi and Yamazaki (2022) based on 90m DEM. Drăguț and Eisank's
 275 results include three levels; here we present results of their level 2 (RefData 3) and level 3 (RefData 4) classification.

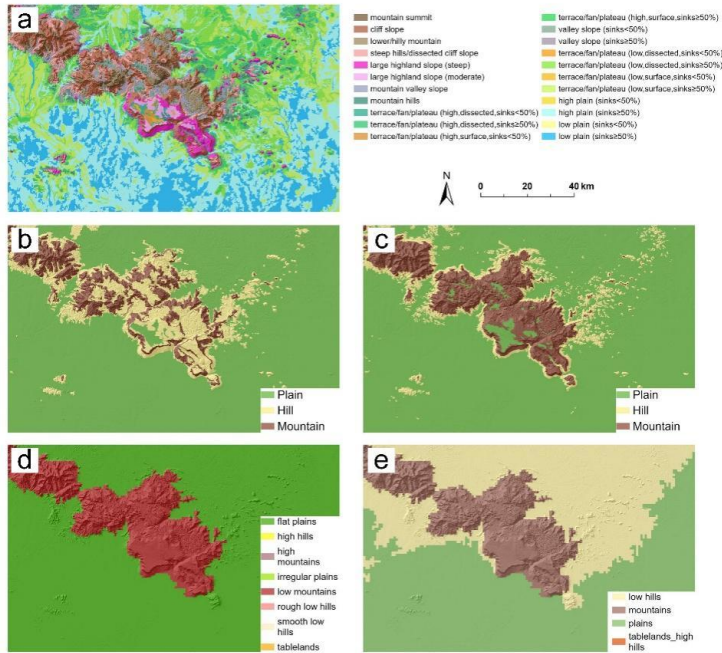


276

277 **Figure 7. Comparison between the GBLU and the Global Mountain Biodiversity Assessment (GMBA) projects.**

278 We conducted a more detailed comparison for mountain regions using the Global Mountain Biodiversity Assessment (GMBA)
279 (Snehlage et al., 2022) as reference data. The GMBA dataset contains three subsets using the DEM with spatial resolutions of 1000
280 m, 1000 m and 250 m to generate global mountain maps. These three datasets (e.g., K1, K2 and K3) are produced by analyzing the
281 morphological derivatives, using a moving neighbourhood analysis window for relief, elevation, and slope (Kapos et al., 2000;
282 Karagulle et al., 2017; Körner et al., 2011). That similar indicators are used in the associated classification and mapping processes
283 indicates the comparability of the GMBA and the GBLU datasets, although due to differences in the category settings among the
284 GBLU and the GMBA datasets, the comparison in this study focused only mountains. As shown in Figure 7, the GBLU dataset
285 clearly outperforms the other three datasets in depicting mountain details, especially in representing valleys. This can be seen in
286 Figures 7a-h, whereby the K1, K2 and K3 data exhibits separated upland blocks in mountainous regions with complex and intense
287 terrain variations, and fails to represent continuous valleys.

288 Due to differences in classification systems and indices, it is challenging to conduct further quantitative comparisons between
289 GBLU and other results. To facilitate comparison between these datasets, we merged some classes in the datasets to maintain
290 classification consistency. For example, we merged mountain summit and cliff slope sections into 'mountain' as per merging criteria
291 described in Table A2. Overall, GBLU results are consistent with other systems in terms of the macroscopic landform patterns. The
292 merged results indicate that Iwahashi and Yamazaki's dataset performs better in representing plains boundaries and their shapes.



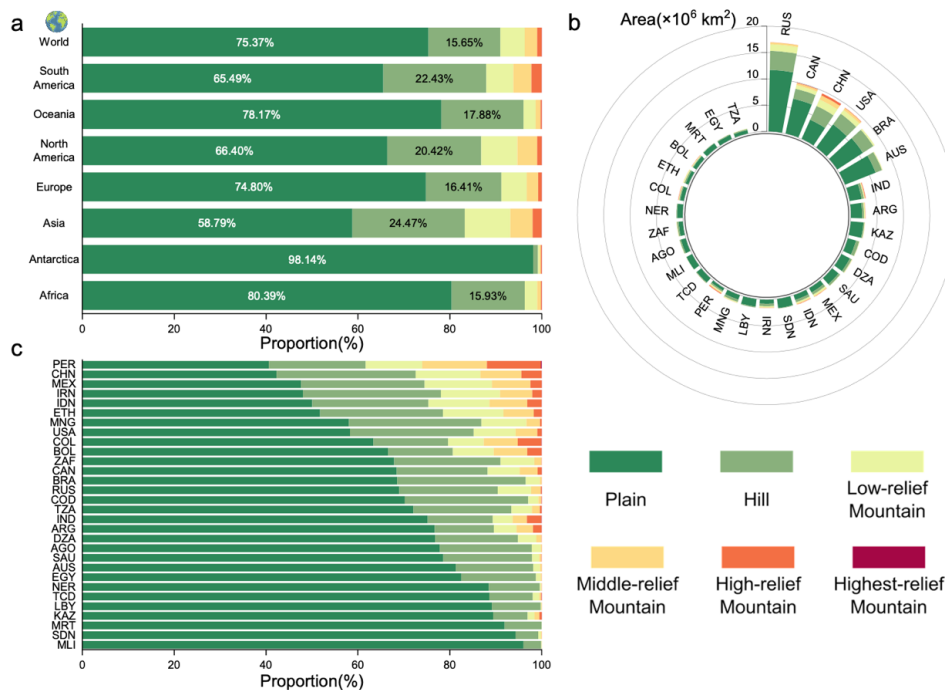
293

294 **Figure 8. Classification result of the GBLU for an existing landform mapping dataset in the Amazon River basin.**

295 **a** Iwahashi and Yamazaki (2022) original result; **b** adjusted Iwahashi and Yamazaki ,2022 result through merging landform

296 classes; **c** GBLU result; **d** Drăguț and Eisank (2012) result (level 3); **e** Drăguț and Eisank, 2012 result (level 2).

297 **3.4 Global landform composition**



298



299 **Figure 9. Area and proportional area statistics at continental and national scales.** **a** Proportion of primary landforms on each
300 continent. **b** Area of primary landform types in the top 30 countries ranked by area. **c** Proportion of primary landform types in the
301 top 30 countries ranked by area. Full names of countries listed can be found in Table A3.

302 We have used a cell size of 500 m x 500 m to accurately assess the proportions of primary landforms across continents
303 worldwide, thereby yielding insights into their spatial variations. The findings indicate that approximately 75% of the global land
304 area comprises plains, while some 16% consists of hills, with the remaining portion classified as mountains (Figure 9a). In terms of
305 the distribution of landform composition, Asia exhibits a very distinctive pattern, since plains cover only 59% of its land area, the
306 lowest among all continents, while there is a significantly higher proportion of hills and mountains, consistent with its pronounced
307 topographic diversity. Compared to the global average, the presence of continental marginal mountain chains results in a
308 significantly lower proportion of plains, and correspondingly higher proportion of mountains, in both North and South America.
309 Indeed, South America has very substantial areas of high relief mountains, while Africa is distinguished by the dominance of
310 extensive plains.

311 We further conducted a comprehensive analysis of landform types and their proportions at the national and regional scale
312 across all countries and regions worldwide to reveal patterns of variation. Figure 9b illustrates the proportion of primary landform
313 types in the top 30 countries ranked by area, while Figure 9c depicts the standardized proportion of the landform types within these
314 countries, sorted based on the proportion of plains. China's diverse and rugged topography is evident in its significantly high
315 proportion of mountains, while Peru contains the lowest proportion of plains, as mountainous terrain there occupies over 60% of its
316 land area.

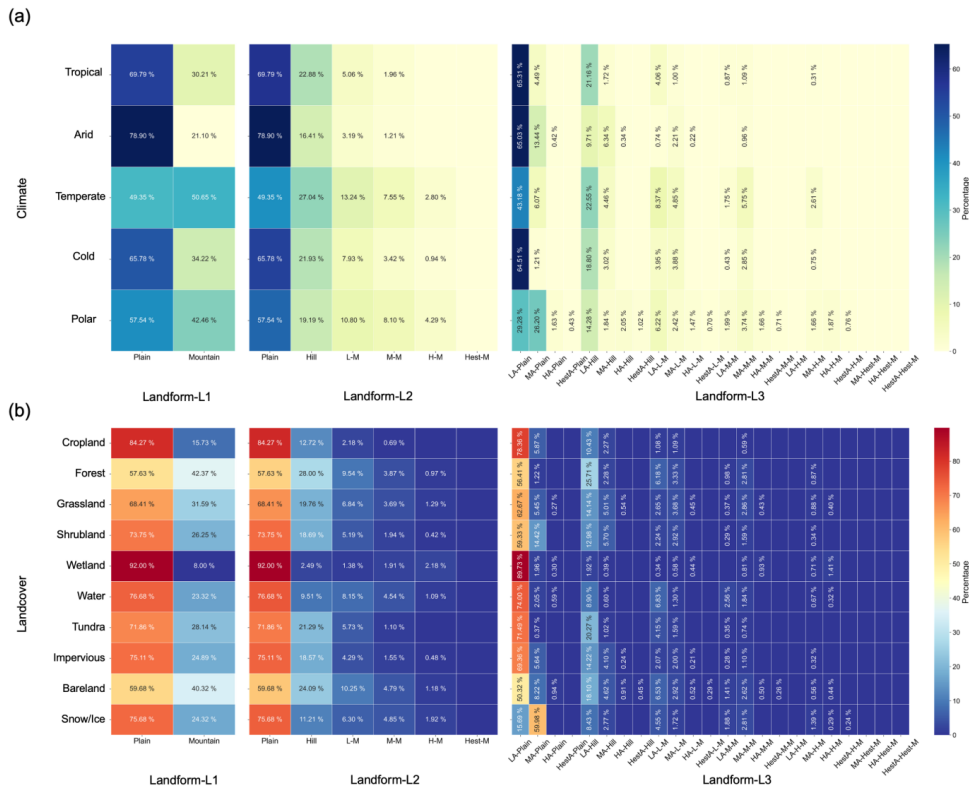
317 **3.4 Dataset usage note**

318 In this section, we highlight the results of experiments performed to analyse the relationship between landforms, climate and
319 land cover to highlight the potential applications of GBLU. Based on the high resolution landform classes provided by GBLU, we
320 can explore the complex and in-depth relationships between landforms, climate, and land cover. The climate data is the widely used
321 1-km Köppen-Geiger climate classification maps in 1991–2020 (Beck et al., 2023) and the land cover data is from FROM-GLC
322 30m in 2017 (Yu et al., 2013).

323 The enhanced resolution and detail of the GBLU enables subtle variations in the Earth's surface to be captured, which is highly
324 valuable in understanding interactions between geomorphology and other factors. As shown in Figure 10, landform distribution in
325 temperate zones suggests a unique blend of climatic conditions and geomorphologic processes, fostering a diverse array of landforms.
326 In the climatic zones of tropical, arid, and cold regions, we observe that low-altitude plains and hills are most prominent. For polar
327 areas, a larger proportion of the area is located at higher altitudes than in other climate zones. Regarding land cover analysis
328 (excluding the South Polar area), cropland occupies 84.27% of plains and 15.73% of mountains, yielding useful insights for
329 analyzing cultivated land productivity. Meanwhile, forests and bare land are more prevalent in mountains, more especially in hills.



330 Additionally, the percentage of many ecologically significant biomes, such as forests, grasslands, wetlands, tundra, and water bodies,
 331 in plains and mountainous regions has been brought up to date. This is potentially valuable for assessing the quality of ecological
 332 environments and carbon stocks.



333
 334 **Figure 10. Relationship of landform types to climate and land cover.** (a) and (b) show the proportions of the three classes of
 335 landform types in different climatic and land cover regions respectively. Values less than 0.2% are not labeled with numbers.

336 The GBLU provided in this work has obvious applications in geomorphology but also in other fields and can, moreover, play
 337 a fundamental role in supporting the identification of landforms that incorporates complex semantics. For example, identification
 338 of a landscape element as ‘tableland’ is complex, differs between disciplines, and requires that both morphological and evolutionary
 339 characteristics be accounted for. The GBLU can be integrated with additional observations to map the occurrence and distribution
 340 of tablelands through the delineation of segments that are elevated, flat, and surrounded by steep escarpments. There is also
 341 significant potential for the application of GBLU to other fields (such as geology, hydrology and ecology) focusing on the natural
 342 environment. For example, for ecologists, biodiversity distribution across different landform regions is one of the most significant
 343 issues and central to understanding the nature of ecosystem change. At the regional scale, contrasting geomorphological conditions
 344 are known to promote isolation of biological populations, influencing community structure and function, as well as evolution.
 345 Meanwhile, the interaction between geomorphology and biogeography may result in complex biogeomorphological dynamics. The
 346 feedback between physical, ecological and evolutionary components constituting biogeomorphological systems is an important



347 element of the evolution of the Earth's surface.

348 **4. Dataset access**

349 Global Basic Landform Units (GBLU v1.0) is stored in the Deep-time Digital Earth Geomorphology platform and Zenodo
350 (Yang et al., 2024; <https://doi.org/10.5281/zenodo.13187969>). The data are stored in Esri shapefile format using the coordinate
351 system WGS84. Total size of the dataset is 150GB, with 6,849,306 independent landform blocks. In order to facilitate application,
352 we employed a $1^\circ \times 1^\circ$ grid to tile the data for storage, with 25,252 file tiles in all. We distinguish the types of landform units by
353 coding attributes of the elements. Additionally, we provide a rasterized dataset (at 30m resolution) using the coordinate system of
354 WGS84. Values of the cells represent the codes of L3 types. In the attribute table, field “code0” is the landform type code of the
355 first level, field “code1” is the landform type code of the second level and field “code2” is the landform type code of the L3.

356 **5. Conclusion**

357 This study provides a novel global landform classification dataset (GBLU) with a resolution of 1 arc-second
358 (approximately 30 m). In this study, we propose a novel framework for global landform mapping to significantly improve
359 the quantitative evaluation of geomorphological features. The key output is the release of the GBLU dataset that is suited to
360 applications across multiple disciplines, including geography, geology, ecology, and hydrology. Global-scale analysis of attributes
361 within the GBLU reveals the composition and distribution of global landforms that enables comparison between regions and
362 continents. The results emphasize the notable heterogeneity of Asia in general, and of China in particular, in terms of
363 geomorphological diversity. The GBLU outperforms previous datasets in expressing landform details, providing an
364 opportunity to investigate the Earth's natural resources. The resolution of the GBLU is similar to that of the current
365 mainstream remote sensing data, which makes combined use of the data relatively simple. We believe that this dataset
366 can provide abundant and detailed geomorphological information for the field of earth sciences, facilitating further
367 advancements in related research.



Appendix A

Table A1. Classification of global basic landform types





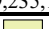

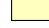




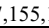



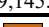
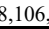





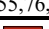
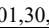




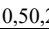






L1	Code	Colors (RGB)	L2	Code	Colors (RGB)	L3	Code	Colors (RGB)			
Plain	1	 129,168,0	Plain	11	 76,115,0	Low-altitude plain	111	 112,168,0			
						Middle-altitude plain	112	 209,235,152			
						High-altitude plain	113	 237,242,179			
						Highest-altitude plain	114	 213,217,164			
Mountain	2	 255,255,190	Hill	21	 240,242,148	Low-altitude hill	211	 230,216,106			
						Middle-altitude hill	212	 220,191,75			
						High-altitude hill	213	 217,155,110			
						Highest-altitude hill	214	 170,141,117			
			Low-relief Mountain	22	 168,112,0	Low-relief Mountain	22	 168,112,0	Low-altitude low-relief mountain	221	 209,145,28
									Middle-altitude low-relief mountain	222	 198,106,20
									High-altitude low-relief mountain	223	 237,122,24
									Highest-altitude low-relief mountain	224	 244,100,18
			Middle-relief Mountain	23	 137,65,47	Middle-relief Mountain	23	 137,65,47	Low-altitude middle-relief mountain	231	 253,120,25
									Middle-altitude middle-relief mountain	232	 255,76,0
									High-altitude middle-relief mountain	233	 201,30,9
									Highest-altitude middle-relief mountain	234	 220,0,0
			High-relief Mountain	24	 86,20,24	High-relief Mountain	24	 86,20,24	Low-altitude high-relief mountain	241	 193,119,120
									Middle-altitude high-relief mountain	242	 110,50,20
									High-altitude high-relief mountain	243	 114,4,9
									Highest-altitude high-relief mountain	244	 115,0,0
			Highest-relief Mountain	25	 255,255,255	Highest-relief Mountain	25	 255,255,255	Middle-altitude highest-relief mountain	252	 156,156,156
									High-altitude highest-relief mountain	253	 225,225,225
									Highest-altitude highest-relief mountain	254	 255,255,255



Table A2. Merging the GBLU results to enable comparison with the results of Iwahashi and Yamazaki.

	Terrain22	Gcluster15	Sinks	legend
Mountain	1	2	1,0	Mountain summit
	2	3	1,0	Cliff slope
	3	13	1,0	Lower/hilly mountain
	4	12	1,0	Steep hills/dissected cliff slope
	5	5	1,0	Large highland slope (steep)
	6	4	1,0	Large highland slope (moderate)
	7	14	1,0	Mountain valley slope
	8	10	1,0	Moderate hills
Hill	9*	11	0	Terrace/fan/plateau (high, dissected, Sinks < 50%)
	10	11	1	Terrace/fan/plateau (high, dissected, Sinks ≥ 50%)
	11	7	0	Terrace/fan/plateau (high, surface, Sinks < 50%)
	12	7	1	Terrace/fan/plateau (high, surface, Sinks ≥ 50%)
	13 ^{xc}	8	0	Valley slope (Sinks < 50%)
	14	8	1	Valley slope (Sinks ≥ 50%)
Plain	15 ^{xc*}	9	0	Terrace/fan/plateau (low, dissected, Sinks < 50%)
	16	9	1	Terrace/fan/plateau (low, dissected, Sinks ≥ 50%)
	17 ^{xc*}	6	0	Terrace/fan/plateau (low, surface, Sinks < 50%)
	18	6	1	Terrace/fan/plateau (low, surface, Sinks ≥ 50%)
	19 ^{xc*}	1	0	High plain (Sinks < 50%)
	20	1	1	High plain (Sinks ≥ 50%)
	21 ^{xc*}	15	0	Low plain (Sinks < 50%)
	22	15	1	Low plain (Sinks ≥ 50%)

Table A3. Countries' names and their abbreviations.

NAME	Abbreviations
Russian Federation	RUS
Canada	CAN
Peoples Republic of China	CHN
United States of America	USA
Federative Republic of Brazil	BRA
Commonwealth of Australia	AUS
Republic of India	IND
Argentina	ARG
Republic of Kazakhstan	KAZ
Democratic Republic of Congo	COD
Democratic People	DZA
Kingdom of Saudi Arabia	SAU
United States of Mexico	MEX
Republic of Indonesia	IDN
Republic of the Sudan	SDN
Islamic Republic of Iran	IRN
Great Socialist People	LBY
Mongolia	MNG
Republic of Peru	PER
Republic of Chad	TCD
Republic of Mali	MLI
Angola	AGO
Republic of South Africa	ZAF
Republic of Niger	NER
Republic of Colombia	COL
Federal Democratic Republic of Ethiopia	ETH
Republic of Bolivia	BOL
Islamic Republic of Mauritania	MRT
Arab Republic of Egypt	EGY
United Republic of Tanzania	TZA



376 **Author contribution**

- 377 Xin Yang, Guoan Tang and Michael Meadows designed the study.
378 Xin Yang, Sijin Li, Junfei Ma, Yang Chen and Xingyu Zhou performed the analysis.
379 Xin Yang and Sijin Li wrote the first version of the manuscript.
380 Fayuan Li, Liyang Xiong and Chenghu Zhou coordinated the work and reviewed the manuscript.
381 Sijin Li, Junfei Ma, Yang Chen and Xingyu Zhou assisted with quality control and reviewed the manuscript.
382 All the authors contributed to the final version of the manuscript.

383 **Competing interests**

- 384 The authors declare that they have no conflict of interest.

385 **References**

- 386 Amatulli, G., Domisch, S., Tuanmu, M.-N., Parmentier, B., Ranipeta, A., Malczyk, J., and Jetz, W.: A suite of global, cross-scale
387 topographic variables for environmental and biodiversity modeling, *Sci Data*, 5, 180040, <https://doi.org/10.1038/sdata.2018.40>,
388 2018.
389 Beck, H. E., McVicar, T. R., Vergopolan, N., Berg, A., Lutsko, N. J., Dufour, A., Zeng, Z., Jiang, X., van Dijk, A. I., and Miralles,
390 D. G.: High-resolution (1 km) Köppen-Geiger maps for 1901–2099 based on constrained CMIP6 projections, *Scientific data*, 10,
391 724, <https://doi.org/10.1038/s41597-023-02549-6>, 2023.
392 Drăguț, L. and Blaschke, T.: Automated classification of landform elements using object-based image analysis, *Geomorphology*, 81,
393 330–344, <https://doi.org/10.1016/j.geomorph.2006.04.013>, 2006.
394 Drăguț, L. and Eisank, C.: Object representations at multiple scales from digital elevation models, *Geomorphology*, 129, 183–189,
395 <https://doi.org/10.1016/j.geomorph.2011.03.003>, 2011.
396 Drăguț, L. and Eisank, C.: Automated object-based classification of topography from SRTM data, *Geomorphology*, 141–142, 21–
397 33, <https://doi.org/10.1016/j.geomorph.2011.12.001>, 2012.
398 Dramis, F.: Geomorphological mapping for a sustainable development, *Journal of Maps*, 1, 53–55,
399 <https://doi.org/10.4113/jom.2009.1084>, 2009.
400 Dyba, K. and Jasiewicz, J.: Toward geomorphometry of plains—Country-level unsupervised classification of low-relief areas (Poland),
401 *Geomorphology*, 413, 108373, <https://doi.org/10.1016/j.geomorph.2022.108373>, 2022.
402 Evans, I. S.: Geomorphometry and landform mapping: What is a landform?, *Geomorphology*, 137, 94–106,
403 <https://doi.org/10.1016/j.geomorph.2010.09.029>, 2012.
404 Florinsky, I. V.: An illustrated introduction to general geomorphometry, *Progress in Physical Geography: Earth and Environment*,
405 41, 723–752, <https://doi.org/10.1177/0309133317733667>, 2017.
406 Gallant, A. L., Brown, D. D., and Hoffer, R. M.: Automated mapping of Hammond's landforms, *IEEE geoscience and remote*
407 *sensing letters*, 2, 384–388, <https://doi.org/10.1109/LGRS.2005.848529>, 2005.
408 Hammond, E. H.: Small-Scale Continental Landform Maps, *Annals of the Association of American Geographers*, 44, 33–42,
409 <https://doi.org/10.1080/00045605409352120>, 1954.
410 Hawker, L., Uhe, P., Paulo, L., Sosa, J., Savage, J., Sampson, C., and Neal, J.: A 30 m global map of elevation with forests and
411 buildings removed, *Environ. Res. Lett.*, 17, 024016, <https://doi.org/10.1088/1748-9326/ac4d4f>, 2022.
412 Hugenholtz, C. H., Levin, N., Barchyn, T. E., and Baddock, M. C.: Remote sensing and spatial analysis of aeolian sand dunes: A
413 review and outlook, *Earth-Science Reviews*, 111, 319–334, <https://doi.org/10.1016/j.earscirev.2011.11.006>, 2012.



- 414 Iwahashi, J. and Pike, R. J.: Automated classifications of topography from DEMs by an unsupervised nested-means algorithm and
415 a three-part geometric signature, *Geomorphology*, 86, 409–440, <https://doi.org/10.1016/j.geomorph.2006.09.012>, 2007.
- 416 Iwahashi, J. and Yamazaki, D.: Global polygons for terrain classification divided into uniform slopes and basins, *Prog Earth Planet*
417 *Sci*, 9, 33, <https://doi.org/10.1186/s40645-022-00487-2>, 2022.
- 418 Iwahashi, J., Kamiya, I., Matsuoka, M., and Yamazaki, D.: Global terrain classification using 280 m DEMs: segmentation, clustering,
419 and reclassification, *Prog Earth Planet Sci*, 5, 1, <https://doi.org/10.1186/s40645-017-0157-2>, 2018.
- 420 Jasiewicz, J. and Stepinski, T. F.: Geomorphons — a pattern recognition approach to classification and mapping of landforms,
421 *Geomorphology*, 182, 147–156, <https://doi.org/10.1016/j.geomorph.2012.11.005>, 2013.
- 422 Kapos, V., Rhind, J., Edwards, M., Price, M., Ravilious, C., and Butt, N.: Developing a map of the world’s mountain forests., *Forests*
423 *in sustainable mountain development: a state of knowledge report for 2000*, Task Force For. Sustain. Mt. Dev., 4–19,
424 <https://doi.org/10.1079/9780851994468.0004>, 2000.
- 425 Karagulle, D., Frye, C., Sayre, R., Breyer, S., Aniello, P., Vaughan, R., and Wright, D.: Modeling global Hammond landform regions
426 from 250-m elevation data, *Transactions in GIS*, 21, 1040–1060, <https://doi.org/10.1111/tgis.12265>, 2017a.
- 427 Karagulle, D., Frye, C., Sayre, R., Breyer, S., Aniello, P., Vaughan, R., and Wright, D.: Modeling global Hammond landform regions
428 from 250-m elevation data, *Transactions in GIS*, 21, 1040–1060, <https://doi.org/10.1111/tgis.12265>, 2017b.
- 429 Körner, C., Paulsen, J., and Spehn, E. M.: A definition of mountains and their bioclimatic belts for global comparisons of biodiversity
430 data, *Alp Botany*, 121, 73–78, <https://doi.org/10.1007/s00035-011-0094-4>, 2011.
- 431 Li, S., Xiong, L., Tang, G., and Strobl, J.: Deep learning-based approach for landform classification from integrated data sources of
432 digital elevation model and imagery, *Geomorphology*, 354, 107045, <https://doi.org/10.1016/j.geomorph.2020.107045>, 2020.
- 433 Li, S., Xiong, L., Hu, G., Dang, W., Tang, G., and Strobl, J.: Extracting check dam areas from high-resolution imagery based on the
434 integration of object-based image analysis and deep learning, *Land Degrad Dev*, 32, 2303–2317, <https://doi.org/10.1002/ldr.3908>,
435 2021.
- 436 MacMillan, R. A. and Shary, P. A.: Landforms and landform elements in geomorphometry, *Developments in soil science*, 33, 227–
437 254, [https://doi.org/10.1016/S0166-2481\(08\)00009-3](https://doi.org/10.1016/S0166-2481(08)00009-3), 2009.
- 438 Martins, F. M. G., Fernandez, H. M., Isidoro, J. M. G. P., Jordán, A., and Zavala, L.: Classification of landforms in Southern Portugal
439 (Ria Formosa Basin), *Journal of Maps*, 12, 422–430, <https://doi.org/10.1080/17445647.2015.1035346>, 2016.
- 440 Maxwell, A. E. and Shobe, C. M.: Land-surface parameters for spatial predictive mapping and modeling, *Earth-Science Reviews*,
441 226, 103944, <https://doi.org/10.1016/j.earscirev.2022.103944>, 2022.
- 442 Pennock, D. J., Zebarth, B. J., and De Jong, E.: Landform classification and soil distribution in hummocky terrain, Saskatchewan,
443 Canada, *Geoderma*, 40, 297–315, [https://doi.org/10.1016/0016-7061\(87\)90040-1](https://doi.org/10.1016/0016-7061(87)90040-1), 1987.
- 444 Shumack, S., Hesse, P., and Farebrother, W.: Deep learning for dune pattern mapping with the AW3D30 global surface model, *Earth*
445 *Surface Processes and Landforms*, 45, 2417–2431, <https://doi.org/10.1002/esp.4888>, 2020.
- 446 Smith, B. and Mark, D. M.: Geographical categories: an ontological investigation, *International Journal of Geographical Information*
447 *Science*, 15, 591–612, <https://doi.org/10.1080/13658810110061199>, 2001.
- 448 Smith, B. and Mark, D. M.: Do Mountains Exist? Towards an Ontology of Landforms, *Environ Plann B Plann Des*, 30, 411–427,
449 <https://doi.org/10.1068/b12821>, 2003.
- 450 Snethlage, M. A., Geschke, J., Ranipeta, A., Jetz, W., Yoccoz, N. G., Körner, C., Spehn, E. M., Fischer, M., and Urbach, D.: A
451 hierarchical inventory of the world’s mountains for global comparative mountain science, *Sci Data*, 9, 149,
452 <https://doi.org/10.1038/s41597-022-01256-y>, 2022.
- 453 Tadono, T., Ishida, H., Oda, F., Naito, S., Minakawa, K., and Iwamoto, H.: Precise Global DEM Generation by ALOS PRISM,
454 *ISPRS Annals of the Photogrammetry, Remote Sensing and Spatial Information Sciences*, II–4, 71–76,



- 455 <https://doi.org/10.5194/isprsannals-ii-4-71-2014>, 2014.
- 456 Xiong, L., Li, S., Tang, G., and Strobl, J.: Geomorphometry and terrain analysis: Data, methods, platforms and applications, Earth-
457 Science Reviews, 104191, <https://doi.org/10.1016/j.earscirev.2022.104191>, 2022.
- 458 Yang, X., Li, S., Ma, J., Chen, Y., Zhou, X., Zhou, C., Meadows, M., Li, F., Xiong, L., & Tang, G.: Global Basic Landform Units
459 (GBLU) datasets v1.0 - raster format (1.0) [Data set]. Zenodo. <https://doi.org/10.5281/zenodo.13187969>, 2024.
- 460 Yu, L., Wang, J., and Gong, P.: Improving 30 m global land-cover map FROM-GLC with time series MODIS and auxiliary data
461 sets: a segmentation-based approach, International Journal of Remote Sensing, 34, 5851–5867,
462 <https://doi.org/10.1080/01431161.2013.798055>, 2013.
- 463 Zhou, C. H., Cheng, W. M., Qian, J. K., Li, B. Y., and Zhang, B. P.: Research on the classification system of digital land
464 geomorphology of 1: 1000000 in China, Journal of Geo-Information Science, 11, 707–724,
465 <https://doi.org/10.3724/SP.J.1047.2009.00707>, 2009.